35

AAS 93-191

THE GRAVITY PROBE B "NIOBIUM BIRD" EXPERIMENT: VERIFYING THE DATA REDUCTION SCHEME FOR ESTIMATING THE RELATIVISTIC PRECESSION OF EARTH-ORBITING GYROSCOPES

Hirohiko Uematsu*, Bradford W. Parkinson†, James M. Lockhart‡ and Barry Muhlfelder‡

Gravity Probe B (GP-B) is a relativity gyroscope experiment begun at Stanford University in 1960 and supported by NASA since 1963. This experiment will check, for the first time, the relativistic precession of an Earth-orbiting gyroscope that was predicted by Einstein's General Theory of Relativity, to an accuracy of 1 milliarcsecond per year or better. A drag-free satellite will carry four gyroscopes in a polar orbit to observe their relativistic precession. The primary sensor for measuring the direction of gyroscope spin axis is the SQUID (superconducting quantum interference device) magnetometer. The data reduction scheme designed for the GP-B program processes the signal from the SQUID magnetometer and estimates the relativistic precession rates. We formulated the data reduction scheme and designed the Niobium bird experiment to verify the performance of the data reduction scheme experimentally with an actual SQUID magnetometer within the test loop. This paper reports the results from the first phase of the Niobium bird experiment, which used a commercially available SQUID magnetometer as its primary sensor, and addresses the issues they raised. The first phase resulted in a large, temperature-dependent bias drift in the SQUID electronics, which showed the need to implement a temperature-insensitive design and a temperature regulation scheme.

INTRODUCTION

The Gravity Probe B (GP-B) experiment is designed to check the relativistic precession of an Earth-orbiting gyroscope (Ref. 1, 2). It is one of the most rigorous experiments ever attempted by NASA because of the precision demands of the measurements. Dr. Frank McDonald, former NASA Chief Scientist, described the project this way: "I consider this the most challenging test we'll undertake in this millennium. For the first time, NASA will have gone out to check one of the fundamental forces in nature." The GP-B experiment will check two previously untested aspects of Einstein's theory of general relativity, geodetic and frame-dragging precession. According to general relativity, if a gyroscope is launched into a polar orbit at an altitude of 650 kilometers (Ref. 3), it will undergo a geodetic precession of about 6.6 arcseconds per year in the

* Mr. Uematsu is a Ph.D. candidate in the Aeronautics and Astronautics Department at Stanford University, Stanford, California 94305.

† Dr. Parkinson is a tenured Professor in the Aeronautics and Astronautics Department and W. W. Hansen Experimental Physics Laboratory of Stanford University and the Program Manager of the Stanford Relativity Gyroscope Experiment, Stanford, California 94305.

‡ W. W. Hansen Experimental Physics Labs, Stanford University, Stanford, Califorinia 94305-4085.

north-south direction and a frame-dragging precession of about 0.042 arcsecond per year in the east-west direction (see Fig. 1). The primary objective of the GP-B program is to measure these relativistic precession rates to an accuracy of 1 milliarcsecond per year or better over the one- to two-year mission.

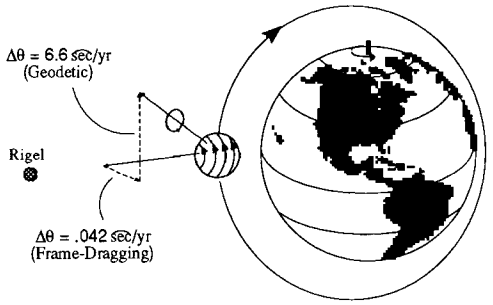

Fig. 1. Relativistic Precession Rates of an Earth-Orbiting Gyroscope

The sensor used to measure the direction of gyroscope spin axis is a dc SQUID (superconducting quantum interference device) magnetometer (Ref. 4), which uses a superconductive loop with two Josephson junctions. Figure 2 is a simplified signal flow chart for the GP-B program. The SQUID magnetometer measures the spin direction onboard, and the digitized signal is sent down to the ground station. There the data reduction scheme processes the signal from the satellite and estimates the relativistic precession rates. Thus, construction of a SQUID magnetometer with a high signal-to-noise ratio and high resolution and optimization of the data reduction scheme are the two keys to the success of this project. We designed the Niobium bird experiment to accomplish these two tasks within one test environment.

The Niobium bird experiment uses a SQUID magnetometer within the test loop (see Fig. 3) to verify the performance of the data reduction scheme. In this process, the

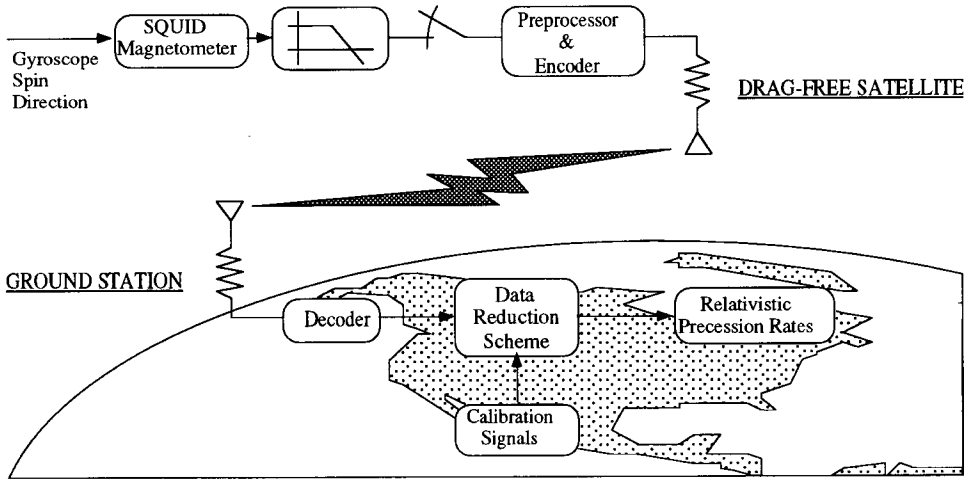

Fig. 2. Simplified Signal Flow Diagram of the Gravity Probe B Program

computerized truth model* that we have compiled simulates a science signal, which a D-to-A converter transforms to an analog signal. The analog signal is injected into the SQUID magnetometer, which measures the local magnetic field created by the signal. An A-to-D converter then digitizes the output of the SQUID magnetometer through an anti-alias lowpass filter. The data reduction scheme** receives the digitized measurement and processes the data to estimate the relativistic precession rates. The estimated rates are then compared with the true values stored in the truth model, and the estimation error is evaluated to verify the performance of the data reduction scheme. The objectives of the Niobium bird experiment are:

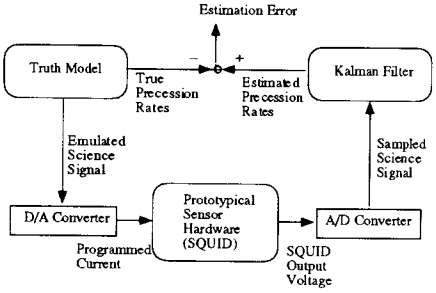

Fig. 3. Conceptual Diagram of the Niobium Bird Experiment

1. Experimental verification of the data reduction scheme
2. Completion of the error budget
3. Refinement of hardware requirements
4. Construction of the prototypical SQUID readout system

In the first phase of the experiment, we attained the first three objectives with a commercially available dc SQUID magnetometer. The following sections detail the Niobium bird experiment and the results of its first phase.

READOUT SYSTEM FOR THE SCIENCE MISSION

The readout system for the GP-B science mission measures the direction of the gyroscope spin axis very precisely without disturbing the gyroscope. It consists of three major parts: a telescope, a superconducting gyroscope, and a dc SQUID magnetometer. The telescope's axis, which is aligned with the satellite's axis of symmetry, points in the optical direction of the guide star Rigel and establishes the reference direction from which the precession of the gyroscope spin axis is measured. The GP-B drag-free satellite carries four gyroscopes made of quartz, each coated by a thin layer of niobium. Liquid helium stored in the satellite cools these gyroscopes to 1.8 Kelvin, and the niobium becomes superconductive. When boiled-off helium gas spins up these gyroscopes, each gyroscope generates a magnetic dipole, called a London moment, because of the superconductive coating. The London moment is aligned with the instantaneous spin axis of the gyroscope, changing its direction as the gyroscope precesses. The London moment is inductively coupled to the pickup loop, which is

* The truth model is a C program compiled on a Sun Sparcstation 330 with SunOS version 4.1.

** The data reduction scheme is another C program compiled on a Sun Sparcstation 330 with SunOS version 4.1.

located around the gyroscope at its equator (see Fig. 4). Any change in the direction of the London moment induces a current in the pickup loop, which in turn changes the magnetic flux within the SQUID loop. The SQUID senses the induced current in the pickup loop, and the output of the SQUID electronics is a voltage proportional to the angle between the spin axis and the pickup loop. The SQUID magnetometer is a relatively new technology, used by the GP-B program as a primary sensor to resolve the precession angle to 0.1 milliarcsecond. Since the SQUID technology is the heart of the GP-B program, it is essential to test the sensor's performance and the data reduction scheme at the same time.

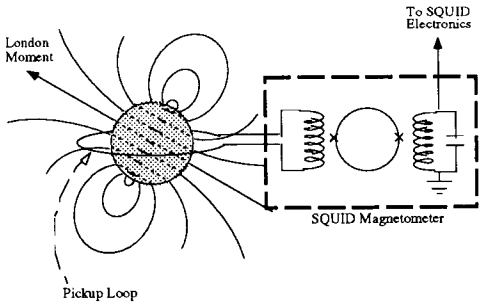

Fig.4. Diagram ofthe SQUID Readout System for the Science Mission

SYNTHESIS OF THE DATA REDUCTION SCHEME

We developed the data reduction scheme for the GP-B program to estimate the relativistic precession rates from the SQUID readout. X. Qin (Ref. 5) initially developed the two-step Kalman filters for the GP-B project. The filtering process consists of two steps, each using a different Kalman filter. For this experiment, the two-step Kalman filters give better insight into the estimator states and have a faster processing speed than a single-step Kalman filter. We reformulated Qin's two-step filter to further increase the processing speed. The following sections explain the formulation of the step 1 and step 2 filters.

Measurement

The step 1 filter takes two measurements: a science signal‡ from the SQUID magnetometer and a roll phase measurement from a star blipper. The science signal contains the relativistic precession terms and is given by the following equation:

$$y = C_G\left[(NS_S + \lambda_1)\sin\psi_r - (EW_S + \lambda_2)\cos\psi_r\right] + b + n \qquad (1)$$

where

$\psi_r \equiv \psi_{rc} + \delta\psi_r$: satellite roll phase

$NS_S \equiv -(\Omega_G t + NS_0) - \alpha r_x/R_{es} + \kappa R_{es} r_x/r_{es}(r_{es} - r_z)$: north-south static term

$EW_S \equiv -(-\Omega_F t\cos\delta_R + EW_0) - \alpha r_y/R_{es} + \kappa R_{es} r_y/r_{es}(r_{es} - r_z)$: east-west static term

λ_1, λ_2: two components of aberration error in the celestial north and celestial east directions, respectively

R_{es}: astronomical unit

‡ The output signal of the SQUID magnetometer, which we call the *science signal*, is proportional to the angle between the gyroscope spin axis and the pickup loop.

r_x, r_y, r_z: three components of the Sun-to-Earth vector in the celestial north, celestial east, and guide star directions, respectively

$$r_{es} \equiv \sqrt{r_x^2 + r_y^2 + r_z^2}$$

Note that the measurement is modulated by the roll phase of the GP-B satellite. The measurement equation (Eq. 1) contains the following nine unknown parameters:

Ω_G:	geodetic precession rate (arcseconds per year)
Ω_F:	frame-dragging precession rate (arcseconds per year)
EW_0:	east-west initial misalignment of gyroscope spin axis (arcseconds)
NS_0:	north-south initial misalignment of gyroscope spin axis (arcseconds)
α:	parallax coefficient
κ:	deflection of starlight coefficient
C_G:	readout scale factor for gyroscope (volts per arcsecond)
b:	readout bias for gyroscope (volts)
$\delta\psi_r$:	phase error for satellite roll (radians)

Among the unknown parameters, the most important are the relativistic precession rates, Ω_G and Ω_F. The two-step Kalman filters estimate the nine unknown parameters from the science signal sampled during the one- to two-year mission. The two aberration terms, λ_1 and λ_2, are determined by the position and velocity of the observer and are known to an accuracy of 0.07 milliarcsecond or better (Ref. 6). Thus, we use these terms to calibrate the scale factor C_G and the roll phase error $\delta\psi_r$ during the step 1 filtering.

Figure 5 shows the simulated science signal using Eq. 1 over three orbits. We assumed a unity scale factor for this simulation, and the vertical axis indicates the angle between the gyroscope's spin axis and the pickup loop in arcseconds. Each orbit takes about 93 minutes, but the science signal is available for about 61 minutes during each orbit because of the occultation of the guide star Rigel. When the satellite moves behind the Earth where the view of Rigel is blocked, the pointing error increases from 20 milliarcseconds to 2 arcseconds in rms (Ref. 7). Since the direction of the gyroscope's spin axis is measured with respect to the telescope axis, the large pointing error corrupts the SQUID readout during the occultation, and the estimation error by the data reduction scheme becomes too large to be useful information. We call this period *Rigel invalid* because the Rigel is not visible from the satellite and call the rest of the orbit, during which the Rigel is visible, *Rigel valid.* The data reduction scheme processes the SQUID readout during Rigel valid and discards the signal during Rigel invalid. Note that the science signal is modulated at the roll frequency, which has a period of 10 minutes, and is also modulated at the orbital frequency, which is indicated by the modulation of the sinusoidal amplitude.

The two-step Kalman filter uses the spectral separation principle to divide the estimation process into two stages: step 1 and step 2 filtering (see Fig. 6). Note that the two terms in Eq. 1, NS_S and EW_S, comprise constant terms, linear terms in time, and annually varying terms. Thus, we can approximate them as constant over one orbital period. During the one-year mission, the satellite will orbit 5400 times around the Earth; we have as many step 1 filters as orbits. Each step 1 filter processes the science signal

sampled during one orbit and estimates the slowly varying terms as constant parameters. Thus, the input signals for the step 1 filters are the science signal and the roll phase measurement, and the output from the step 1 filters consists of the estimation of slowly varying terms and their expected covariance matrices. Once all the step 1 filters finish estimating the slowly varying terms, the step 2 filter processes the output from the step 1 filters to estimate eight of the nine unknown parameters, i.e., all but the readout bias.

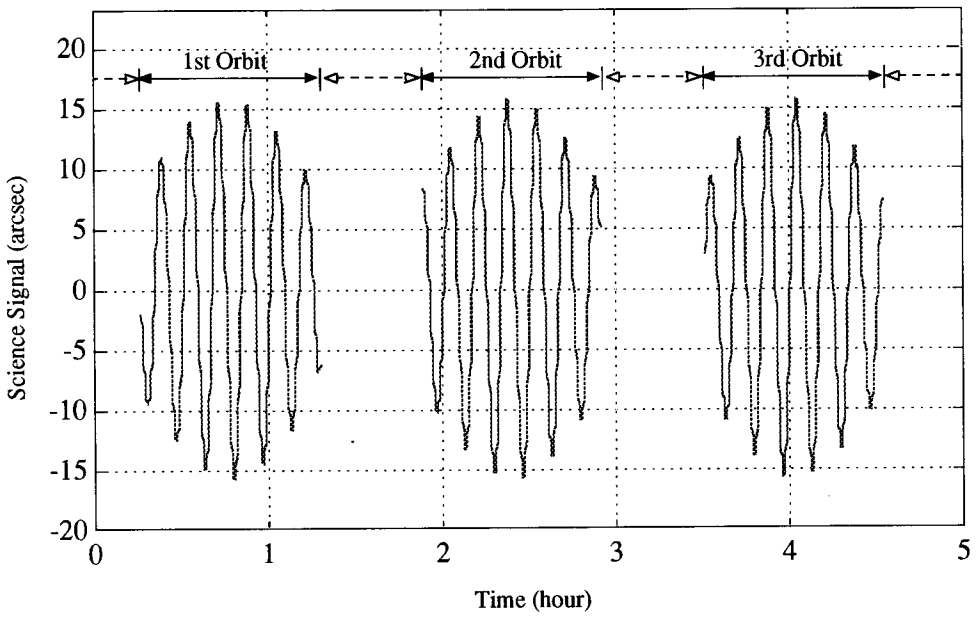

Fig. 5. Science Signal from a SQUID Magnetometer Over Three Orbits
◄——► "Rigel Valid" Period, ◄- - -► "Rigel Invalid" Period

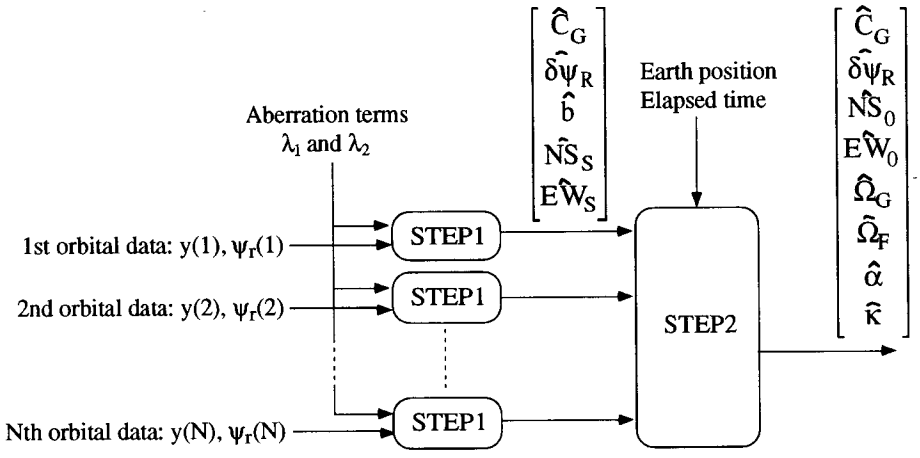

Fig. 6. Simplified Diagram of the Two-Step Filters

Step 1 Filtering

As Fig. 5 shows, the science signal is modulated at the roll frequency, and the step 1 filters demodulate the science signal to dc and annually modulated signals. The state vector for each step 1 filter is as follows:

$$x_1 = \begin{bmatrix} C_G & \delta\psi_r & b & NS_S & EW_S \end{bmatrix}^T \tag{2}$$

Each parameter is assumed to be constant over one orbit; thus, the process model for the step 1 filter is given by the following equation:

$$\begin{aligned} x_1(k+1) &= \Phi_1 x_1(k) + \Gamma_1 w_1(k) \\ y(k) &= h(x_1(k)) + n_k \end{aligned} \tag{3}$$

where

$$\Phi_1 = I_{5\times5},\ \Gamma_1 = \begin{bmatrix} I_{3\times3} \\ \varnothing_{2\times3} \end{bmatrix}_{5\times3}$$

$$h(x_1) \equiv C_G\left[(NS_S + \lambda_1)\sin(\psi_{rc} + \delta\psi_r) - (EW_S + \lambda_2)\cos(\psi_{rc} + \delta\psi_r)\right] + b$$

The measurement equation is a nonlinear function of the state elements as given by Eq. 1. We formulated each step 1 filter as an extended Kalman filter, and the measurement equation was linearized around an *a priori* estimate as follows:

$$\begin{aligned} z(k) &= H_1(k)x_1(k) + n_k \\ &= y(k) - h(\bar{x}_1(k)) + H_1(k)\bar{x}_1(k) + n_k \end{aligned} \tag{4}$$

where

$$H_1(k) \equiv \left.\frac{dh(x)}{dx}\right|_{x=\bar{x}_1(k)}$$

With the measurement equation given in a linear form, we used the SRIF (square root information filter) algorithm (Ref. 8) to formulate the step 1 filter.

Step 2 Filtering

The step 2 filter further demodulates the output of the step 1 filters from the annual frequency to dc. The step 2 filter takes the output of the step 1 filter as measurements, as shown in Fig. 6. The state vector for the step 2 filter is as follows:

$$x_2 = \begin{bmatrix} C_G & \delta\psi_r & NS_0 & EW_0 & \Omega_G & \Omega_F & \alpha & \kappa \end{bmatrix}^T \tag{5}$$

Each component is constant, and the measurements are linear in the state elements. Hence, the process model for the step 2 filter is given by the following equation:

$$x_2(k+1) = \Phi_2 x_2(k) + \Gamma_2 w_2(k)$$
$$\hat{\rho}_1(k) = H_2 x_2(k) + \tilde{\rho}_1(k) \tag{6}$$

where

$$\hat{\rho}_1(k) = \left[\hat{C}_G(k) \quad \delta\hat{\psi}_r(k) \quad N\hat{S}_S(k) \quad E\hat{W}_S(k)\right]^T$$
$$\tilde{\rho}_1(k) = \left[\tilde{C}_G(k) \quad \delta\tilde{\psi}_r(k) \quad N\tilde{S}_S(k) \quad E\tilde{W}_S(k)\right]^T$$
$$\Phi_2 = I_{8\times8},\ \Gamma_2 = \begin{bmatrix} I_{2\times2} \\ \varnothing_{6\times2} \end{bmatrix}_{8\times2},\ H_2 = \begin{bmatrix} I_{2\times2} & \varnothing_{2\times6} \\ \varnothing_{1\times2} & \partial NS_S/\partial x_2 \\ \varnothing_{1\times2} & \partial EW_S/\partial x_2 \end{bmatrix}_{4\times8}$$
$$\frac{\partial NS_S}{\partial x_2} = \left[0 \quad 0 \quad -1 \quad 0 \quad -t \quad 0 \quad -r_x/R_{es} \quad R_{es}r_x/r_{es}(r_{es}-r_z)\right]$$
$$\frac{\partial EW_S}{\partial x_2} = \left[0 \quad 0 \quad 0 \quad -1 \quad 0 \quad t\cos\delta_R \quad -r_y/R_{es} \quad R_{es}r_y/r_{es}(r_{es}-r_z)\right]$$

Note that the input to the step 2 filter, $\hat{\rho}_1$ in Eq. 6, contains four of the five states of the step 1 filters, C_G, $\delta\psi_r$, NS_S and EW_S. We omitted the estimation of the readout bias from the step 2 filtering because the bias is spectrally separated from the other states, which are modulated at the roll frequency of satellite.

The step 2 filter is a linear filter, whereas the step 1 filters are nonlinear. Thus, the step 1 filtering is more important than the step 2 filtering in the sense that the first-step filters linearize the measurement equation and are more sensitive to the accuracy of the initial estimation error. The next section shows the simulation results from the step 1 and 2 filters.

Results of the Simulation

We verified the step 1 filters and the step 2 filter by simulation before applying them to the actual experimental data. The truth model simulated a science signal equivalent to the signal during a one-year mission, and the data reduction filters processed the simulated signal. We evaluated the final estimation error and the time history of estimation and found that the filters yielded satisfactory accuracy. Results from one Monte-Carlo simulation are presented in this section.

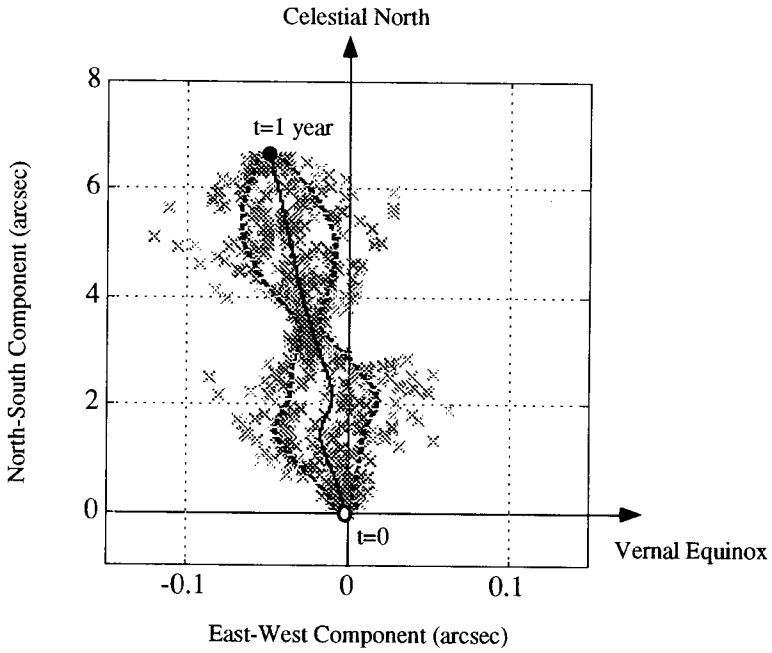

Fig. 7. Results of Step 1 Filtering from the One-Year Simulation: True Values of NS_S and EW_S (Solid Line) Vs. Estimated Values (X's).

Figure 7 shows the results of step 1 filters. The estimates of the north-south component NS_S and the east-west component EW_S are plotted in a plane determined by the directions of the celestial north and the vernal equinox. The origin is located at the observer, i.e., the GP-B satellite. A unit vector that is aligned with the gyroscope's spin axis is projected on the plane. The solid line indicates the trajectory of the gyroscope precession observed with respect to the telescope axis over the one-year mission. The hollow circle represents the two components at the beginning of the mission, and the filled circle represents them at the end of the mission. The x's scattered around the solid line show the estimates from the step 1 filters. Each point represents the estimates of NS_S and EW_S from a step 1 filter. The dotted lines show the envelopes of the expected estimation error (one-sigma rms error). The expected estimation error is minimized at the beginning, in the middle, and at the end of the one-year mission because the annual aberration, which the step 1 filters use as a calibration signal, is modulated at the annual frequency and has maxima at these points. The maximal estimation error is about 100 arcseconds. The north-south and east-west components, NS_S and EW_S, comprise the slowly varying terms such as parallax, deflection of starlight, and relativistic precession, which are now estimated by the step 2 filter.

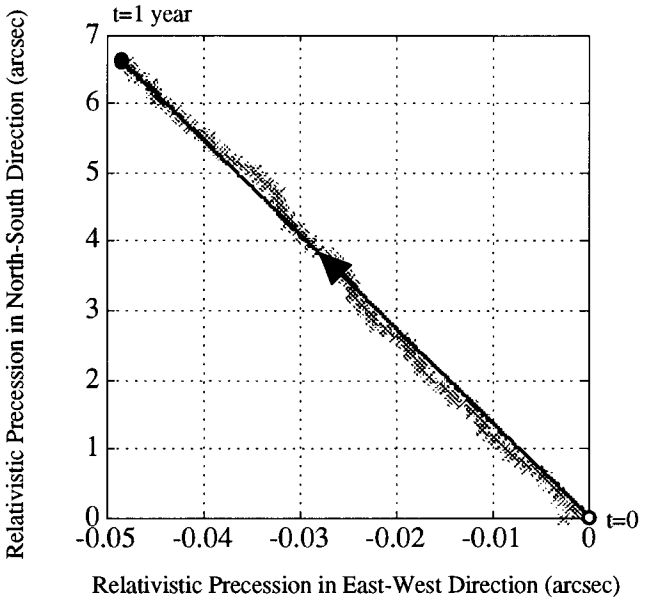

(a) Trajectory of Relativistic Precession - True Values Vs. Estimated Values

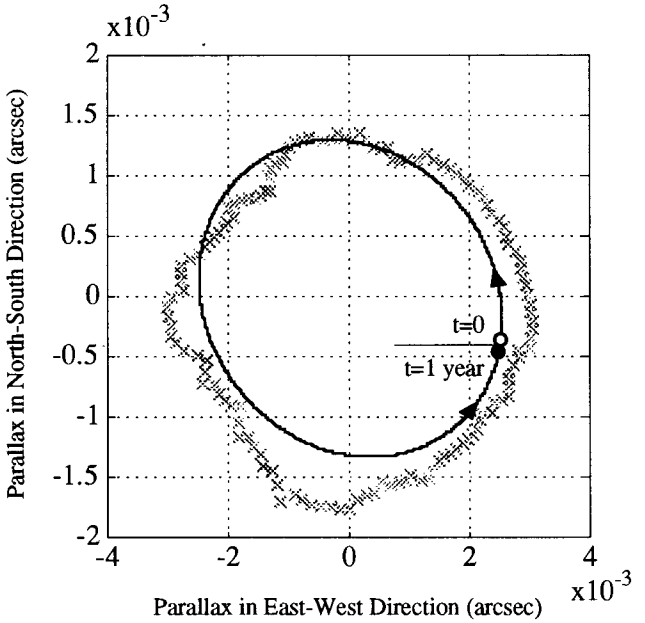

(b) Trajectory of Parallax - True Values Vs. Estimated Values

Fig. 8. Results of Step 2 Filtering from One-Year Simulation:
True Values (Solid Lines) Vs. Estimated Values (X's) of Relativistic Precessoin, Parallax, and Deflection of Starlight (continued on next page).

The step 2 filter processed the estimates from the step 1 filters by treating them as new measurements and estimated the final parameters given in Eq. 5. Figure 8 (a), (b), and (c) show the estimates of the relativistic precession, the parallax, and the deflection of starlight, respectively. Again, the solid lines indicate the true values and the x's indicate the estimated values. The hollow circles represent the true values at the beginning of the mission, and the filled circles represent them at the end of the mission. The north-south component of the relativistic precession is geodetic, and the east-west component is frame-dragging. The other two elements, parallax and deflection of starlight, are modulated at the annual frequency and are as small as the frame-dragging precession. The final estimation errors and the expected rms errors calculated by the step 2 filter are listed in Table 1. For this Monte-Carlo simulation, even though the final estimation error of the parallax was larger than the expected rms error, those of the relativistic precession rates and the deflection of starlight were smaller than or equal to the expected rms error. We ran at least 10 Monte-Carlo simulations and obtained the final estimation errors of Ω_G and Ω_F smaller than 0.5 milliarcsecond per year from each run. Thus, we verified that the two-step filters developed above yielded satisfactory final estimation errors with simulation.

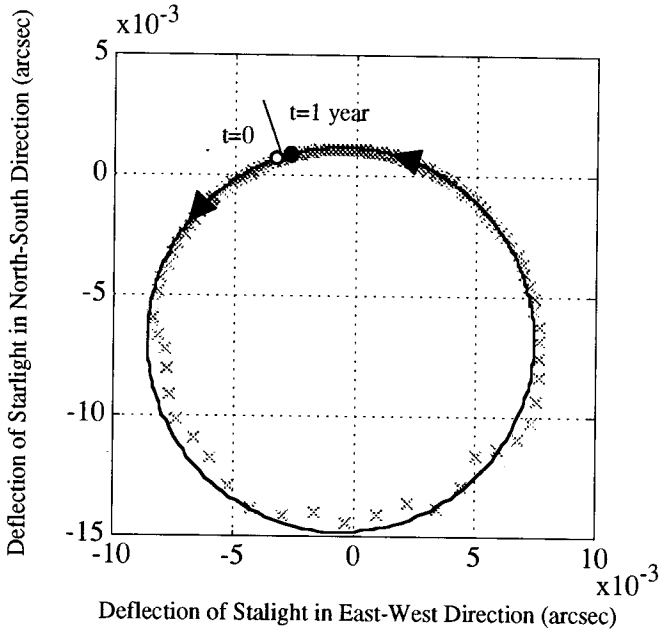

(c) True Values Vs. Estimated Values of Deflection of Starlight

Fig. 8. Results of Step 2 Filtering from One-Year Simulation
True Values (Solid Lines) Vs. Estimated Values (X's) of Relativistic Precession, Parallax, and Deflection of Starlight (continued from previous page).

Table 1. Final Estimation Errors and Expected RMS Errors of A Monte-Carlo Simulation

	Final Estimation Error (milliarcseconds per year)	Expected Estimation Error (1-σ) (milliarcseconds per year)
Ω_G	0.17	0.53
Ω_F	0.14	0.42
α	0.29	0.18
κ	0.12	0.12

NIOBIUM BIRD EXPERIMENT

The Niobium bird experiment has three vital components, as shown in Fig. 3, the truth model, the data reduction scheme, and the SQUID hardware. Figure 9 shows the experimental set-up. The waveform generator outputs current proportional to the simulated science signal. The programmed current is then injected into the SQUID probe, which is immersed in the liquid helium. This programmed current generates a local magnetic field around the probe, and the SQUID magnetometer outputs voltage proportional to the strength of the local magnetic field. The A-to-D converter digitizes the output voltage from the SQUID magnetometer and sends data to the computer. Finally, the data reduction scheme stored in the computer processes the measurement and estimates the relativistic precession rates.

The most important part in the experimental set-up is the cryogenic dewar, which holds up to 80 litters of liquid helium. We installed critical components such as the gyroscope, pickup loop, and SQUID probe in the dewar and kept them superconductive throughout the experiment. The dewar can keep the instruments superconducting for about 3 to 4 weeks. At the bottom of the dewar is a gyroscope coated with niobium. The gyroscope becomes superconducting when it is cooled to 4.2 Kelvin, but it does not create a London moment because it is fixed to the housing. Instead, we have an extra coil, called *calibration coil,* just outside the

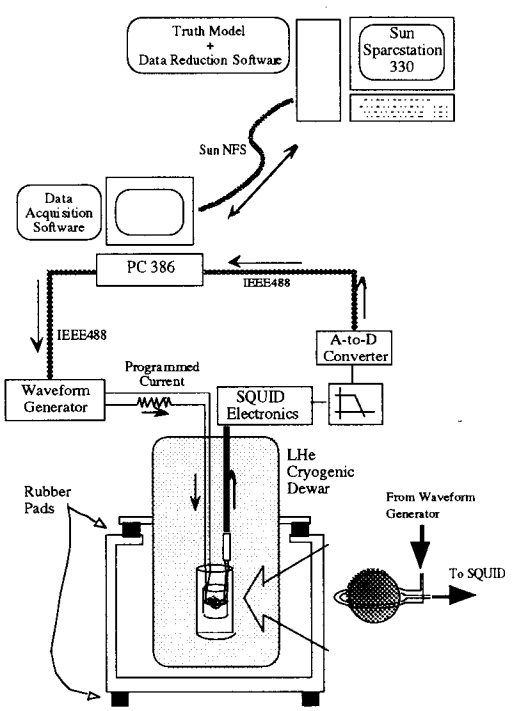

Fig. 9. Niobium Bird Experiment Setup

pickup loop (see Fig. 10). The waveform generator injects the programmed current into the calibration coil. The current creates a magnetic field within the calibration coil, which is inductively coupled to the pickup loop. Thus, any change in the programmed current induces a current in the pickup loop, and the SQUID magnetometer outputs a voltage proportional to the magnetic flux within the pickup loop. The injected current is programmed so that the magnetic field generated inside the pickup loop is equivalent to the London moment of the science mission. Thus, we call the magnetic field created by the programmed current an *artificial London moment.*

The SQUID magnetometer senses the strength of the local magnetic field around the SQUID probe. Hence, it is necessary to control precisely the following functions of the magnetometer when it is installed:

- Shielding of the ambient magnetic field
- Isolation of structural vibration
- Flotation of the electric ground
- Temperature control of the liquid helium

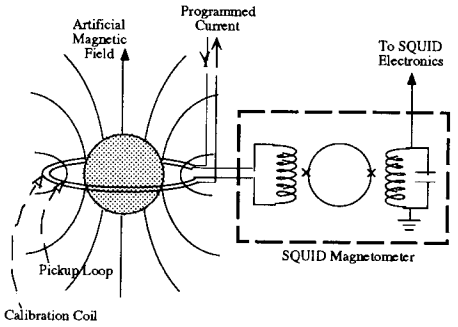

Fig.10. Diagram of the SQUID Readout System for the Niobium Bird Experiment

The ambient magnetic field was shielded by three layers of niobium and one of iron alloy. We hung the dewar from the external structure through rubber pads to isolate structural vibration (see Fig. 9). The SQUID magnetometer is very sensitive to the fluctuation of the power supply, and thus, we had to float the electric ground for the SQUID magnetometer and the D-to-A converter. The dewar itself became the electric ground for these instruments. We also regulated the temperature of the liquid helium with a heater, a PID controller, and a vacuum pump, which kept the helium gas pressure under the atmospheric pressure. Figure 11 shows the control error of the liquid helium; we have successfully regulated the temperature within 2 μK (rms) about the set point, which was 1.93 K. We tested the SQUID magnetometer under the above conditions; the sections that follow present the results of the calibration and the actual experiment.

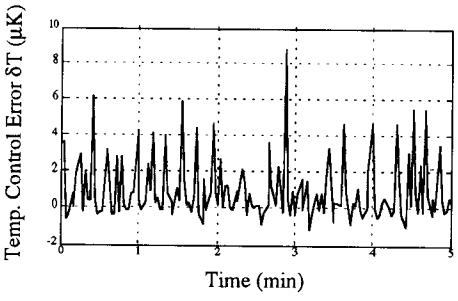

Fig. 11. Control Error of the Temperature of the Liquid Helium Inside the Dewar

CALIBRATION

We calibrated the instruments for the Niobium bird experiment, including the D-to-A converter, SQUID electronics, anti-alias lowpass filter, and A-to-D converter. This section presents the calibration results for the SQUID magnetometer that we used for this experiment.

For the first phase of the Niobium bird experiment, we decided to use a commercially available dc SQUID magnetometer, manufactured by Quantum Design, Inc. We calibrated it with noise power spectral density, bias stability, and scale factor stability. Figure 12 shows the power spectral density of the actual noise of the Quantum Design SQUID and that of a simulated SQUID noise. The data reduction scheme was tuned and verified with the simulated SQUID noise. SQUID generally shows a 1/f spectral density for the lower frequencies, and the corner frequency ranges from 0.1 Hz to 1 Hz. The Quantum Design SQUID exhibited satisfactory noise power at the roll frequency, but also showed $1/f^2$ trend at the lower frequencies. This trend is closely related to the bias drifting of the SQUID readout. Table 2 shows the calibration results of the bias and the scale factor stability. The scale factor satisfied the stability requirement imposed by the Kalman filter, but the bias drift was about 20 times worse than the required limit.

We investigated the dependency of the bias drift on the temperature of the SQUID electronics instead of on that of the liquid helium because the bias drift did not improve even with the temperature control of the liquid helium (see Fig. 11). Figure 13 shows the bias drift of the SQUID readout and the temperature of the SQUID electronics. The bias drift exhibited a strong correlation to the temperature of the electronics with a temperature coefficient of about 1 arcsecond per Kelvin. This correlation imposes new hardware requirements on the design of the SQUID electronics. According to the temperature coefficient of the SQUID electronics manufactured by Quantum Design, we have to regulate the temperature of the electronics within 50 mK (rms) at dc and within 50 μK (rms) at the roll frequency.

Table 2. Stability of Scale Factor and Bias Drift of the SQUID Magnetometer – Requirements Vs. Reality

	Requirements	Experimental Results
Scale Factor Variation	5e–3 %/day	7e–3 %/day
Bias Drift	0.05 arcsecond/day	1 arcsecond/day

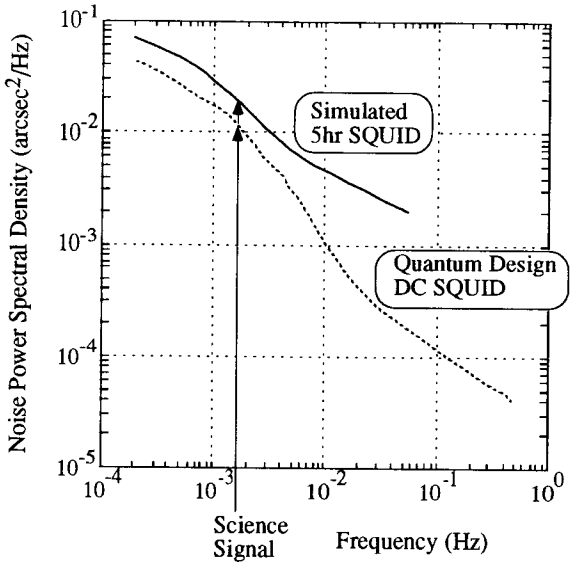

Fig. 12. Power Spectral Density of SQUID Noise: Simulated SQUID Noise (Solid Line) Vs. Quantum Design SQUID Noise (Dotted Line)

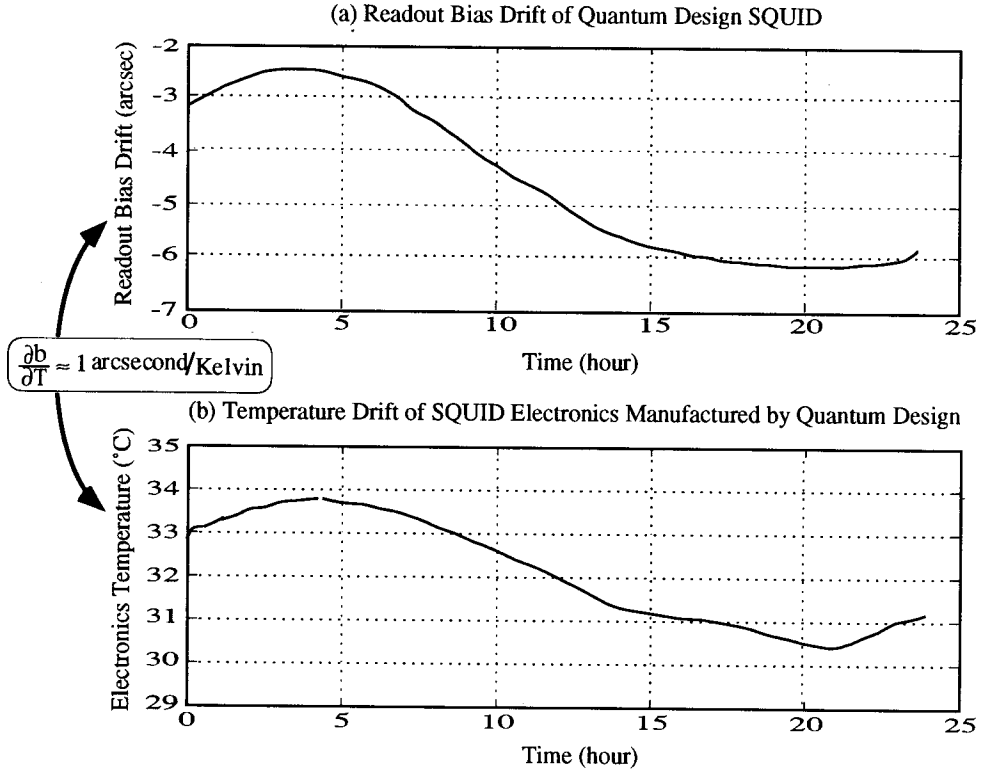

Fig. 13. Dependency of the Readout Bias on the Temperature of SQUID Electronics Manufacutured by Quantum Design: (a) Readout Bias Drift Vs. (b) Temperature Drift

RESULTS

The step 1 filters were tested with the experimental data from the Quantum Design SQUID magnetometer. We did not install the temperature regulation system of the SQUID electronics for this particular test. Thus, the bias of SQUID readout showed a large drift dependent on the electronics temperature. The step 1 filters became unstable when we applied the experimental data because the actual bias drift was much larger than what the process model of Kalman filter assumed (see Table 2). Figure 14 shows experimental results of three step 1 filters, which processed the SQUID data over three orbits; each segment corresponds to one orbit, and the solid lines in Fig. 14 (a) indicate the time history of NS_S estimation error. The dotted lines indicate the time history of the expected estimation errors obtained by propagating covariance matrices. Figure 14 (b) shows the estimation residual of the three step 1 filters. The estimation error overshot outside the expected rms error, and the estimation residual showed divergence. Thus, we had to increase the process noise of the bias state within the Kalman filter to stabilize the filters, which resulted in much larger estimation error. Table 3 shows the expected estimation errors of NS_S and EW_S for the first three orbits after we increased the process noise in the step 1 filters. The second column shows the simulation results, and the third column shows the experimental results. Even though the step 1 filters were stable, the estimation error of NS_S was about seven times worse than the simulation, and that of EW_S was about thirty four times worse. Thus, the final estimation errors of the relativistic precession rates will be about 3.5 milliarcseconds per year for the geodetic precession and about 17 milliarcseconds per year for the frame-dragging precession, which are not acceptable errors for the GP-B experiment.

Table 3. Expected Estimation Error of Step 1 Filter After One Orbit: Simulation Vs. Experiment

	Expected Estimation Error at the End of One Orbit: **Simulation** (arcseconds)	Expected Estimation Error at the End of One Orbit: **Experiment**† (arcseconds)
North-South Component, NS_S	0.018	0.13
East-West Component, EW_S	0.008	0.28

† The major error is due to inadequate thermal control in the SQUID electronics designed and manufactured by Quantum Design. We are currently designing our own SQUID electronics for the science mission, and the new readout system should improve the estimation accuracy by at least two orders of magnitude.

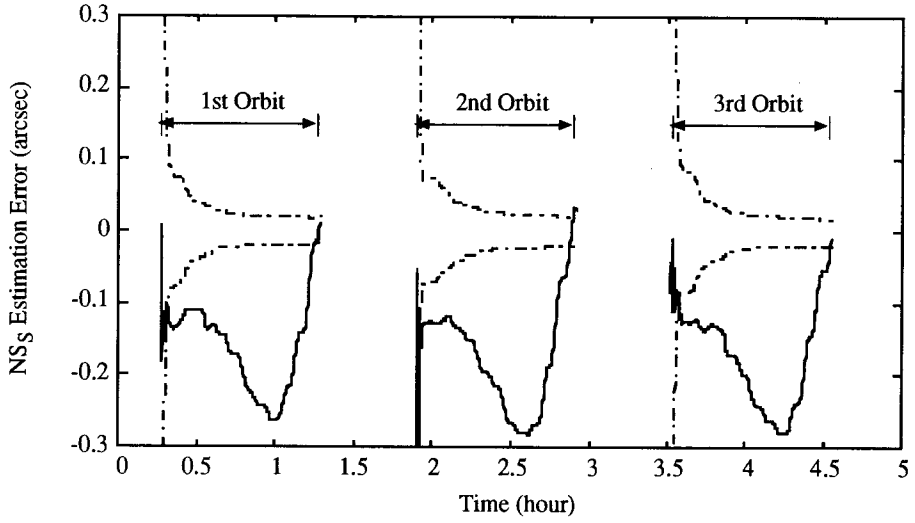

(a) Time History of NS_S Estimation Error Over Three Orbits

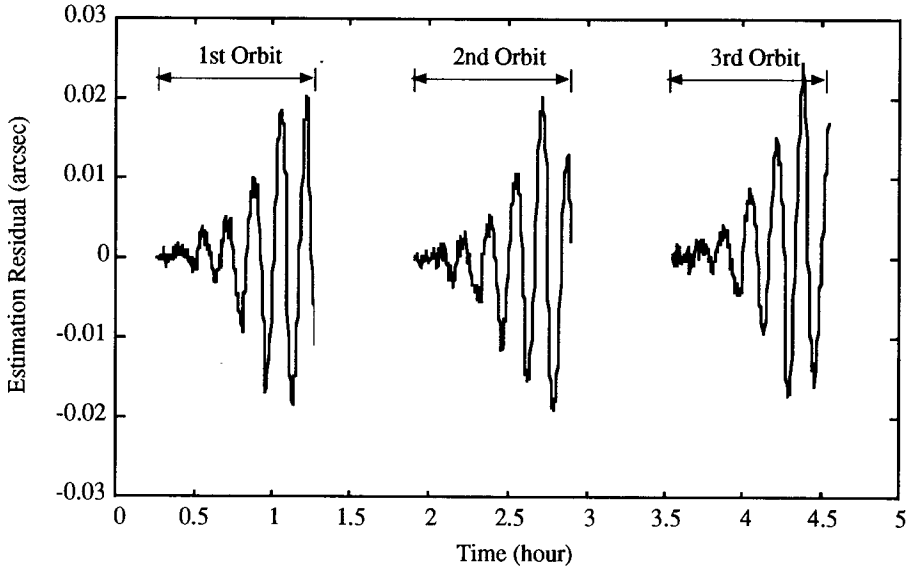

(b) Time History of Estimation Residual of Step 1 Filters Over Three Orbits

Fig. 14. Experimental Results of Step 1 Filtering with Quantum Design SQUID Magnetometer: (a) Time History of the Estimation Error of the North-South Component NS_S, (b) Time History of the Estimation Residual of Three Step 1 Filters

CONCLUSIONS

We developed the two-step Kalman filters for the GP-B program to estimate the relativistic precession rates to an accuracy of 1 milliarcsecond per year or better, and tested them by Monte-Carlo simulations and the Niobium bird experiment. During the Monte-Carlo simulations, the filters yielded the final estimation error of 0.5 milliarcsecond per year or better for the relativistic precession rates. We then tested the filters with the dc SQUID magnetometer manufactured by Quantum Design in the Niobium bird experiment. The Quantum Design SQUID showed satisfactory signal-to-noise ratio at the roll frequency, and its scale factor was stable to 0.007% per day as we expected during the synthesis of Kalman filters. The critical factor in this experiment was the large, temperature-dependent bias drift in the Quantum Design SQUID, which was about twenty times larger than the requirement posed by the data reduction scheme. The Kalman filters became unstable during the first application because of this bias drift. Even though we stabilized the filters by increasing the process noise of the bias state, the final estimation errors of the step 1 filters increased by a factor of seven to thirty four compared with the simulation results. The temperature-dependent bias drift in the Quantum Design SQUID raised new hardware requirements on the SQUID electronics for the science mission. First, the temperature of the SQUID electronics has to be regulated so that the bias drift satisfies the requirement posed by the data reduction scheme. Second, the SQUID electronics has to be designed in a way that it is less sensitive to the ambient temperature.

We completed the first phase of the Niobium bird experiment with the commercially available dc SQUID magnetometer. Now we started developing the second phase, which includes design of a dc SQUID magnetometer for the science mission. From the results we obtained during the first phase, we are pursuing temperature-insensitive design and implementation of temperature regulation system to the new SQUID readout electronics, which will replace the Quantum Design SQUID electronics in the Niobium bird experiment.

ACKNOWLEDGMENTS

This work has been supported under NASA grant # NAS8-36125. I would like to thank James M. Lockhart of the Gravity Probe B program for providing the SQUID magnetometer and helping to establish the Niobium bird experiment.

NOTATION

$I_{n\times n}$: n-by-n identity matrix
$\varnothing_{m\times n}$: m-by-n matrix with zero elements
$\bar{x}$: *a priori* estimation vector
$\hat{x}$: *a posteriori* estimation vector
$\tilde{x}$: *a posteriori* estimation error vector

REFERENCES

[1] L. I. Schiff, "Possible New Experimental Test of General Relativity Theory," *Physical Review Letters* **4**, pp. 215-217 (1960).

[2] C. W. F. Everitt, "The Stanford Relativity Gyroscope Experiment (A): History and Overview," in *Near Zero: New Frontiers of Physics* J. D. Fairbank, J. B. S. Deaver, C. W. F. Everitt, P. F. Michelson, Eds. (W. H. Freeman and Company, New York, 1988), pp. 587-639.

[3] R. Vassar, J. V. Breakwell, C. W. F. Everitt, R. A. VanPatten, "Orbit Selection for the Stanford Relativity Gyroscope Experiment," *J of Spacecraft and Rockets* **19**, pp. 66-71 (1982).

[4] T. V. Duzer, C. W. Turner, *Principles of Superconductive Devices and Circuits* (Elsevier, New York, 1981).

[5] X. Qin, "Data Reduction Analysis for the Stanford Relativity Gyroscope Experiment," Ph.D. Dissertation, Stanford University (1991), SUDAAR 611.

[6] T. G. Duhamel, "Contributions to the Error Analysis in the Relativity Gyroscope Experiment," Ph.D. Dissertation, Stanford University (1984), SUDAAR 540.

[7] N. J. Kasdin, "Precision Pointing Control of the Spinning Gravity Probe B Spacecraft," Ph.D. Dissertation, Stanford University (1991), SUDAAR 606.

[8] G. J. Bierman, *Factorization Methods for Discrete Sequential Estimation*. R. Bellman, Eds., Mathematics in Science and Engineering (Academic Press, Inc., San Diego, CA, 1977), vol. 128.